ADVANCED FUNCTIONAL MATERIALS

Supporting Information

for *Adv. Funct. Mater.*, DOI: 10.1002/adfm.201805684

Organic Bidirectional Phototransistors Based on Diketopyrrolopyrrole and Fullerene

*Frank-Julian Kahle, Tobias Hahn, Tushita Mukhopadhyay, Boregowda Puttaraju, Satish Patil, and Anna Köhler**

Supporting Information

Organic Bidirectional Phototransistors Based on Diketopyrrolopyrrole and Fullerene

Frank-Julian Kahle[1], Tobias Hahn[1], Tushita Mukhopadhyay[2], Boregowda Puttaraju[2], Satish Patil[2], and Anna Köhler[1,3]*

[1] *Soft Matter Optoelectronics, University of Bayreuth, 95440 Bayreuth, Germany*

[2] *Solid State and Structural Chemistry Unit, Indian Institute of Science, Bangalore-560012, India*

[3] *Bayreuth Institute of Macromolecular Science (BIMF), University of Bayreuth, 95440 Bayreuth, Germany*

**anna.köhler@uni-bayreuth.de*

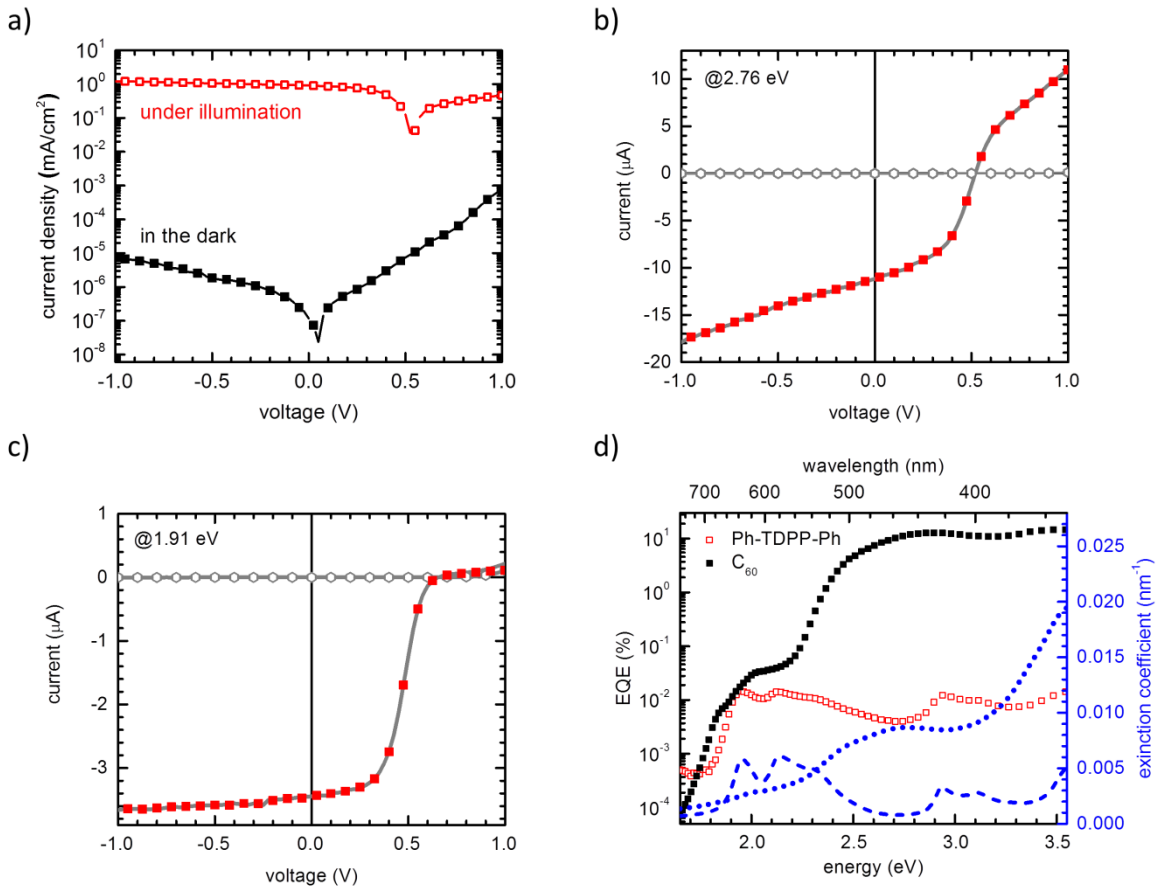

Figure S1: a) Exemplary J-V-characteristic of a Ph-TDPP-Ph/C60 device with MoO_3 interlayer measured under 1 sun illumination (red open symbols) and in the dark (black filled squares). b) I-V-characteristic measured at 7 $\frac{mW}{cm^2}$ and an excitation energy of 2.76 eV. c) Same as in b) but at an excitation energy of 1.91 eV. Dark (light grey circles) and photocurrent contribution (red filled squares) to the total current (grey solid line) are explicitly shown. c) Left axis: EQE spectra of Ph-TDPP-Ph and C_{60} single layer devices measured under short circuit conditions. Right axis: Absorption spectra of Ph-TDPP-Ph (dashed blue) and C_{60} (dotted blue).

Comment on the definition of the photocurrent

In this study, the term "photocurrent" is defined as the difference between the total current measured with and without light exposure. According to Wehenkel et al.[1], the direct identification of the difference between the current under illumination and in the dark with a photogenerated current is only justified, when the voltage drop across the series resistance R_S of the electrodes can be neglected. This is the case for low injection currents which are typical under reverse bias. Under forward bias, however, injection usually dominates the current above V_{oc} and the effective voltage across the active layer may actually be lower due to the voltage drop across R_S. Yet, as in our case the dark current is much lower than the current under illumination, no further correction is needed here.

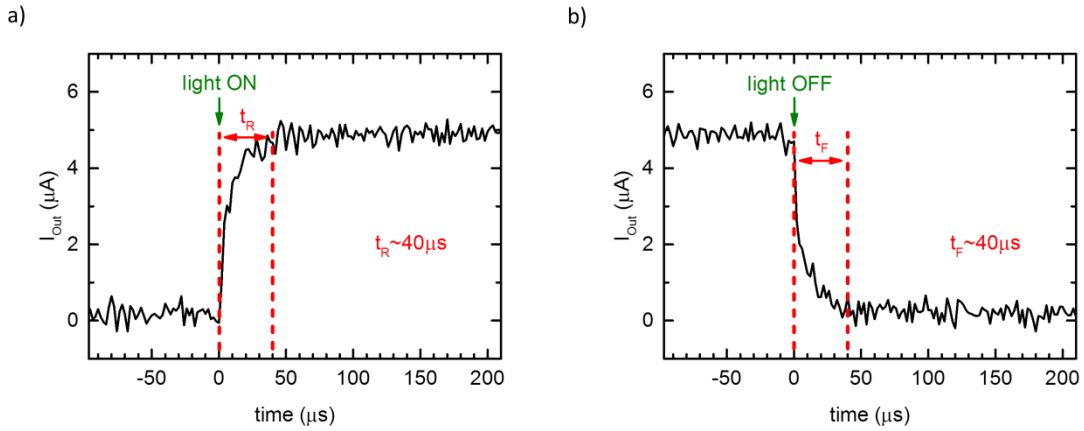

Figure S2: Response times for an AND-Gate when the light is turned a) ON and b) OFF. The total response time is given by the sum of rise (t_R) and fall time (t_F).

Further details about the optoelectronic mechanism

Intensity dependent I-V-measurements

Figure S3a-c display intensity dependent I-V-characteristics of devices with MoO_3 interlayer recorded at a) 3.54 eV, b) 2.76 eV, and c) 1.91 eV, i.e. above and below 2.25 eV, respectively. While the shape of the curves measured at 2.76 eV and 3.54 eV does not change with illumination intensity, a pronounced S-shape emerges with increasing intensity at 1.91 eV. Furthermore, a considerable net photocurrent is present when illuminating the device with 2.76 eV or 3.54 eV light, whereas it is nearly vanishing for 1.91 eV (see also Figure 2b, S1b and S1c).

In order to get an idea about the dissociation processes happening in the device it is convenient to convert the monochromatic I-V-data into field dependent EQE (**Figure S3d**).[2-4] An estimation of the electric field E is simply calculated via $E = \frac{V_{appl} - V_0}{d}$, where V_{appl} is the externally applied voltage, V_0 denotes the compensation voltage and d is the thickness of the active layer of the device. Following the approach of Schwarz et al. presented in Ref. [3] we obtain saturation field strengths F_{Sat} in the range of $3 \cdot 10^4 - 5 \cdot 10^4 \ \frac{V}{cm}$. According to the work of Schwarz et al., F_{Sat} can be regarded as a measure of the ease of dissociation of charge transfer (CT) states at the D/A interface.[3] For 1.91 eV, i.e. below 2.25 eV, we obtain a very well defined saturation regime, as already expected from EQE data, whereas at energies above 2.25 eV an additional field dependence emerges at higher electric fields, implying a further exciton dissociation process. The same observations regarding the shape of the I-V-curves and the saturation field strength for different energies also apply to devices with PEDOT:PSS instead of MoO_3 (**Figure S4**).

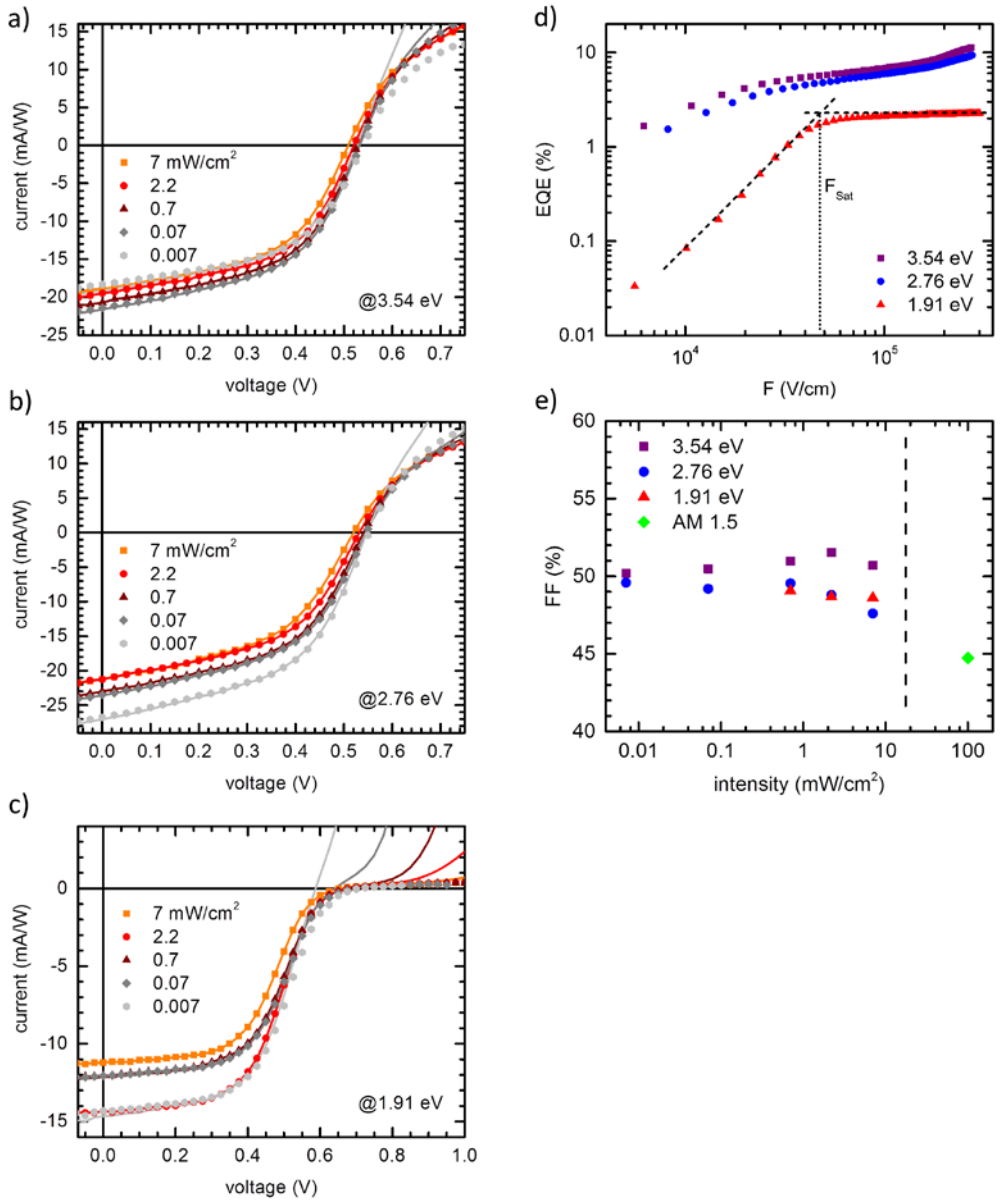

Figure S3: Intensity dependent I-V-characteristics of Ph-TDPP-Ph/C_{60} bilayer devices with MoO_3 interlayer measured at a) 3.54 eV, b) 2.76 eV, and c) 1.91 eV. The respective total currents at the indicated intensities are drawn as solid lines, whereas the associated photocurrents are depicted as filled symbols of the same colour. d) Field dependent EQE for excitation energies of 3.54 eV, 2.76 eV and 1.91 eV. The intersection of the two dashed tangents indicates the saturation field strength F_{Sat}. e) Intensity dependence of the FF for the same energies as in d).

Finally, the degree and kind of recombination present in the device may be addressed via the intensity dependence of the fill factor (FF).[5] The FF as function of illumination intensity is displayed in **Figure S3e** for excitation energies of 3.54 eV, 2.76 eV and 1.91 eV. For reference

also the FF obtained under AM1.5 conditions is given (see also main text). Due to the very low current at 1.91 eV, the FF for the two lowest intensities was omitted, as V_{OC} is largely dominated by the dark current in this case. Overall, we observe only small changes in the range of ± 2 %, meaning that the FF is basically independent of intensity for all three wavelengths. The absolute value is about 50 % up to an intensity of 7 $\frac{mW}{cm^2}$. Under solar conditions (AM1.5) the FF is slightly lower (45 %). Devices with PEDOT:PSS as HIL/HTL feature overall smaller values for FF under both monochromatic illumination as well as sunlight conditions (Figures S1a and **S4b-d**).

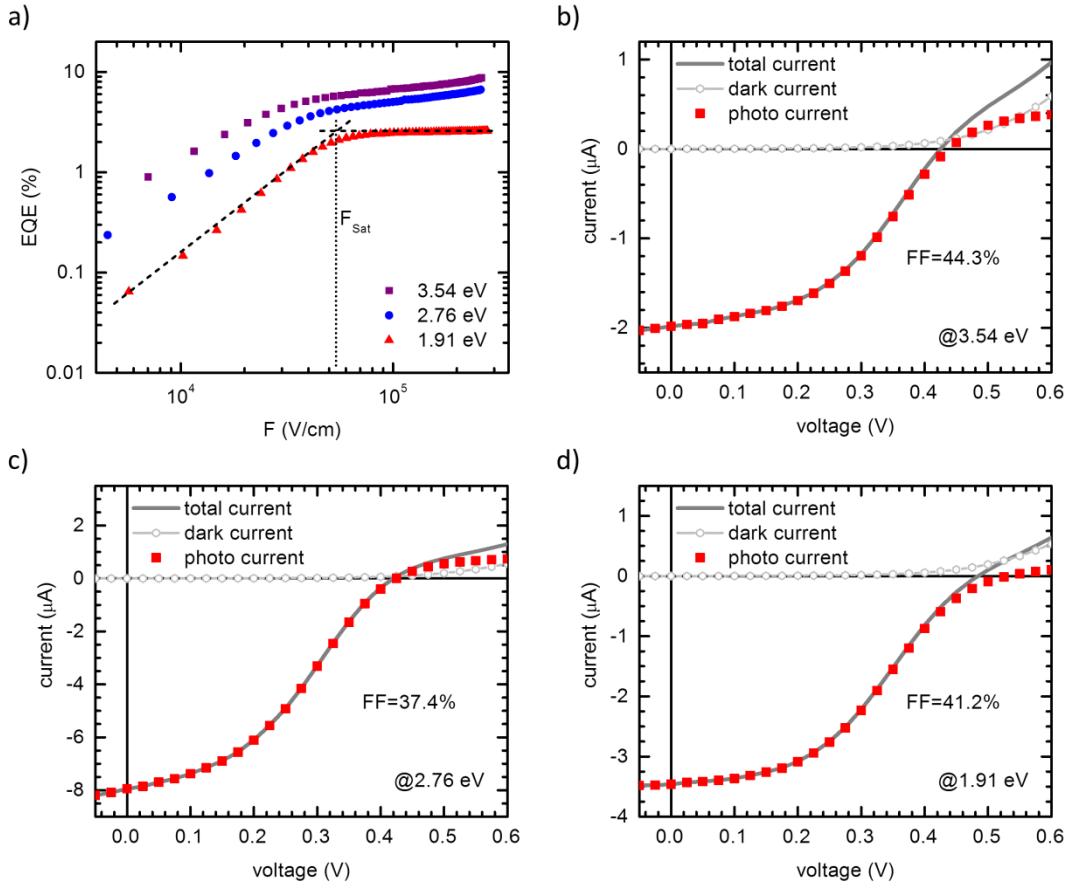

Figure S4: a) Field dependent EQE for excitation energies of 3.54 eV, 2.76 eV and 1.91 eV for PEDOT:PSS/Ph-TDPP-Ph/C_{60} devices. The intersection of the two dashed tangents indicates the saturation field strength F_{Sat}. b) Corresponding I-V-characteristic measured at 7 $\frac{mW}{cm^2}$ and an excitation energy of b) 3.54 eV, c) 2.76 eV, and d) 1.91 eV. Dark (light grey circles) and photocurrent contribution (red filled squares) to the total current (grey solid line) are explicitly shown.

From the presence of a defined saturation regime and the small F_{Sat} derived from field dependent EQE at 1.91 eV, we can conclude that all CT states are easily dissociated at the D/A interface and the resulting charges are separated efficiently. This is a result of good transport properties as well as maybe delocalization of the charge carriers in the donor or the acceptor or even both.[3-4, 6-10] Unlike for 1.91 eV, an additional field dependence appeared at higher electric fields at excitation energies above 2.25 eV. According to Hahn et al. this can be attributed to an additional splitting of CT states generated in the bulk of C_{60}.[11] This autoionization process is also the reason for the considerable EQE observed for C_{60} single layer devices. With this in mind, the EQE spectrum at +1 V can be easily assigned to the intrinsic charge carrier generation in C_{60}.[11] The independence of the FF on illumination intensity for devices with MoO_3 interlayer indicates that no bimolecular recombination is present in these devices.[5]

Presence of a hole injection barrier

When replacing MoO_3 with PEDOT:PSS, the dark current is overall at least two orders of magnitude higher (**Figure S5**). Undoubtedly, this effect is related to the presence of a considerable hole injection barrier in the case of MoO_3.

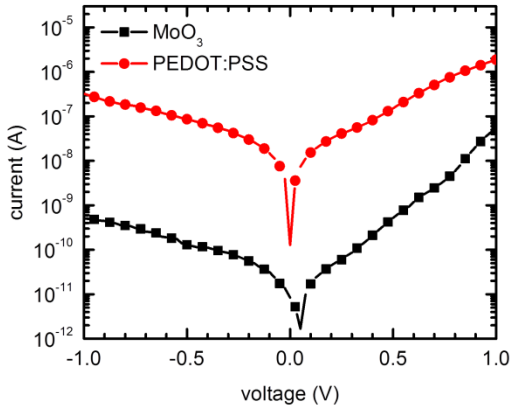

Figure S5: Dark current characteristics of Ph-TDPP-Ph/C_{60} devices with either MoO_3 (black squares) or PEDOT:PSS (red circles) as anode interlayer.

Moreover, the presence of an injection barrier in the case of a MoO_3 interlayer is experimentally verified by the characteristic intensity dependent behavior of the J-V curves measured at 1.91 eV (Figure S3c).[12-13] A similar effect is not observed for energies above 2.25 eV, as in this case the behavior is dominated by a considerable net photocurrent in forward direction that is still present at intensities as low as 0.007 $\frac{mW}{cm^2}$. Both observations, explain the low dark current in

devices with MoO_3 interlayer compared to those with PEDOT:PSS interlayer, where the barrier is obviously considerably lower. The latter is also reflected in the overall smaller EQE (**Figure S6a**) and the lower FF (Figure S4b-d and **S6b**) in samples with PEDOT:PSS, because a larger density of injected charge carriers enhances bimolecular recombination .

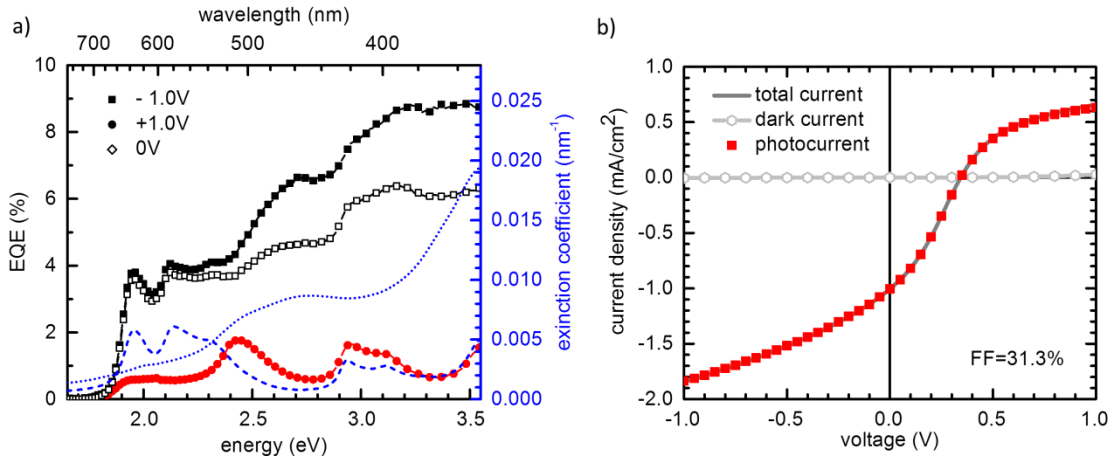

Figure S6: a) Left axis: Series of voltage dependent EQE spectra of PEDOT:PSS/Ph-TDPP-Ph/C_{60}-Devices; Right axis: Absorption spectra of Ph-TDPP-Ph (dashed blue) and C_{60} (dotted blue). b) Exemplary J-V-characteristic of a Ph-TDPP-Ph/C_{60} device with PEDOT:PSS interlayer measured at 1 sun illumination. Dark (light grey circles) and photocurrent contribution (red filled squares) to the total current (grey solid line) are explicitly shown.

Summary

We had seen that

(1) A significant photocurrent in forward direction is only observed for energies above 2.25 eV, i.e. when charge carriers are generated within the C_{60} bulk due to autoionization of CT-states.
(2) Ph-TDPP-Ph does not feature any significant intrinsic photogeneration ability.
(3) Ph-TDPP-Ph[14-16] and C_{60} [17] feature sufficiently good charge transport properties to ensure good extraction and avoid additional losses due to low or imbalanced mobilities between donor and acceptor.[8]
(4) Under reverse bias, dissociation of CT states at the D/A interface is efficient.
(5) A significant hole injection barrier is present in the case of a MoO_3 interlayer, which effectively suppresses the dark current in the devices.

In view of these observations, the presence of a net photocurrent can be explained in terms of an enhanced recombination current close to the cathode and the D/A-interface due to the photoinduced increase of minority charge carrier densities at the respective interface (holes at the cathode, electrons at the acceptor side of the D/A-interface),[1, 18] as discussed in the main text.

In the light of this explanation, the significantly reduced photocurrent at +1V for devices with PEDOT:PSS interlayer (Figure S6a) compared to those with MoO_3 interlayer (Figure 4a) can be attributed to a higher dark injection current for PEDOT:PSS because of a lower injection barrier for holes. This in turn leads to increased bimolecular recombination due to the higher charge carrier density. In contrary, for MoO_3 interlayers, that introduce a larger hole injection barrier, the dark current is much lower resulting in significantly less bimolecular recombination so that photogenerated charge carriers in the C_{60} bulk can effectively contribute to the measured photocurrent.[1] A slightly more detailed discussion of the EQE at +1V of PEDOT:PSS containing devices is given below.

Comment on the EQE spectra recorded at +1V (with PEDOT:PSS interlayer)

The EQE spectrum at +1V follows the absorption of Ph-TDPP-Ph down to about 2.4eV, i.e. close the autoionization threshold of CTS in the C_{60} bulk at 2.25 eV (Figure S6a). Below this energy, the extracted EQE values have to be treated with caution, as the measured current in the dark and under illumination were of the same order. This fact results in larger errors when calculating the photo current from the difference between the illumination current and the dark current, particularly below 2.25 eV.

The fact that the EQE roughly follows the absorption spectrum of Ph-TDPP-Ph indicates the presence of a displacement current that is caused by the recombination of charge carriers, especially electrons, from the C_{60} side at the D/A-interface with excitons generated by photon absorption in the bulk of Ph-TDPP-Ph. The remaining electron from Ph-TDPP-Ph may then be transported to PEDOT:PSS, where it can recombine with an injected hole or be extracted. Consequently, the additional recombination between excitons in Ph-TDPP-Ph and electrons from C_{60} is limited on the one hand by the number of excitons generated in Ph-TDPP-Ph, as well as the number of charges generated from CT states in the C_{60} bulk via autoionization. This mechanism may explain the fact that the additional displacement current only follows the absorption of Ph-TDPP-Ph down to an energy where autoionization of CT states in the C_{60} bulk is still possible.

The remaining contribution below 2.25 eV could be due to exciton diffusion to the D/A-interface or the ITO/MoO_3 electrode and a subsequent (inefficient) splitting, as no significant intrinsic dissociation was observed in single devices of Ph-TDPP-Ph.

Energy levels of Ph-TDPP-Ph and C_{60}

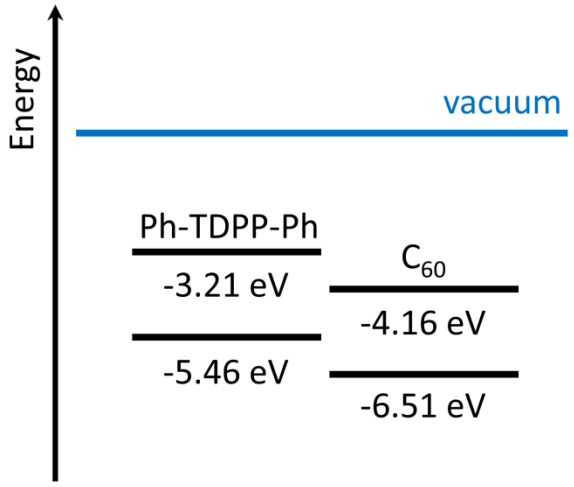

Figure S7: Energy levels of Ph-TDPP-Ph and C_{60}

The variation in frontier molecular orbital energy levels of Ph-TDPP-Ph was investigated by cyclic voltammetry measurements (CV) at a scan rate of 0.1 V/s. Platinum electrodes were used as working and counter electrode; where Ag/ Ag+ have been employed as the reference electrode. Energy levels have been calibrated with respect to an internal standard ferrocene/ferrocenium redox couple. Energy levels of C_{60} are taken from literature and were measured via UPS/IPES.[19]

References

1 D. J. Wehenkel, L. J. A. Koster, M. M. Wienk, R. A. J. Janssen, *Phys Rev B* **2012**, *85*, 125203.
2 T. Hahn, J. Geiger, X. Blase, I. Duchemin, D. Niedzialek, S. Tscheuschner, D. Beljonne, H. Bässler, A. Köhler, *Adv Funct Mater* **2015**, *25*, 1287.
3 C. Schwarz, H. Bässler, I. Bauer, J. M. Koenen, E. Preis, U. Scherf, A. Köhler, *Adv Mater* **2012**, *24*, 922.
4 C. Schwarz, S. Tscheuschner, J. Frisch, S. Winkler, N. Koch, H. Bässler, A. Köhler, *Phys Rev B* **2013**, *87*, 155205.
5 T. Hahn, S. Tscheuschner, F. J. Kahle, M. Reichenberger, S. Athanasopoulos, C. Saller, G. C. Bazan, T. Q. Nguyen, P. Strohriegl, H. Bässler, A. Köhler, *Adv Funct Mater* **2017**, *27*, 1604906.
6 S. Tscheuschner, H. Bässler, K. Huber, A. Köhler, *J Phys Chem B* **2015**, *119*, 10359.
7 S. Athanasopoulos, S. Tscheuschner, H. Bässler, A. Köhler, *J Phys Chem Lett* **2017**, *8*, 2093.
8 W. Tress, K. Leo, M. Riede, *Phys Rev B* **2012**, *85*, 155201.
9 S. Gélinas, A. Rao, A. Kumar, S. L. Smith, A. W. Chin, J. Clark, T. S. van der Poll, G. C. Bazan, R. H. Friend, *Science* **2014**, *343*, 512.
10 B. Bernardo, D. Cheyns, B. Verreet, R. D. Schaller, B. P. Rand, N. C. Giebink, *Nat Commun* **2014**, *5*, 3245.
11 T. Hahn, S. Tscheuschner, C. Saller, P. Strohriegl, P. Boregowda, T. Mukhopadhyay, S. Patil, D. Neher, H. Bässler, A. Köhler, *J Phys Chem C* **2016**, *120*, 25083.
12 W. Tress, in *Organic Solar Cells: Theory, Experiment, and Device Simulation*, Springer, New York 2014, 474.
13 W. Tress, O. Inganäs, *Sol Energ Mat Sol C* **2013**, *117*, 599.
14 R. Könenkamp, G. Priebe, B. Pietzak, *Phys Rev B* **1999**, *60*, 11804.
15 V. D. Mihailetchi, Vol. Doctoral Thesis, University of Gronigen, 2005.
16 B. P. Rand, J. G. Xue, S. Uchida, S. R. Forrest, *J Appl Phys* **2005**, *98*, 124902.
17 A. Pickett, M. Torkkeli, T. Mukhopadhyay, B. Puttaraju, A. Laudari, A. E. Lauritzen, O. Bikondoa, J. Kjelstrup-Hansen, M. Knaapila, S. Patil, S. Guha, *Acs Appl Mater Inter* **2018**, *10*, 19844.
18 W. Tress, in *Organic Solar Cells - Theory, Experiment and Device Simulation*, Springer, New York 2014, 474.
19 F. J. Kahle, C. Saller, S. Olthof, C. Li, J. Lebert, S. Weiß, E. M. Herzig, S. Hüttner, K. Meerholz, P. Strohriegl, A. Köhler, *J Phys Chem C* **2018**, accepted.